

Strain effects on ferroelectric polarization and magnetism in orthorhombic HoMnO_3

Diana Iuşan,^{1,2,*} Kunihiro Yamauchi,^{2,3} Paolo Barone,² Biplab Sanyal,¹ Olle Eriksson,¹ Gianni Profeta,² and Silvia Picozzi²

¹*Department of Physics and Astronomy, Uppsala University, Box 516, 75120 Uppsala, Sweden*

²*Consiglio Nazionale delle Ricerche - Superconducting and Innovative Materials and Devices (CNR-SPIN), 67100 L'Aquila, Italy*

³*Institute of Scientific and Industrial Research (ISIR-SANKEN),*

Osaka University, 8-1 Mihogaoka, Ibaraki, Osaka, 567-0047, Japan

(Dated: June 10, 2018)

Aiming at increasing the ferroelectric polarization in AFM-E ortho- HoMnO_3 , we investigate the in-plane strain effects on both the magnetic configuration and the polarization by means of density functional theory calculations and model Hamiltonian approaches. Our results show that the net polarization is largely enhanced under compressive strain, due to an increase of the electronic contribution to the polarization, whereas the ionic contribution is found to decrease. We identify the electron-lattice coupling, due to Jahn-Teller (JT) distortions, and its response to strain to be responsible for the observed behavior. The JT-induced orbital ordering of occupied $\text{Mn-}e_g^1$ electrons in alternating $3x^2 - r^2/3y^2 - r^2$ orbital states at equilibrium changes to a mixture with $x^2 - z^2/y^2 - z^2$ states under in-plane compressive strain. The asymmetric hopping of e_g electrons between Mn ions along zig-zag spin chains (typical of the AFM-E spin configuration) is therefore enhanced under strain, explaining the large value of the polarization. We reproduce the change in the orbital ordering pattern in a degenerate double-exchange model supplemented with electron-phonon interaction. In this picture, the orbital ordering change is related to a change of the Berry phase of the e_g electrons, which in turn causes an increase of the polarization, whose origin is purely electronic.

PACS numbers: 75.85.+t, 75.50.Ee

I. INTRODUCTION

Orthorhombic rare-earth manganites RMnO_3 , which crystalize in the $Pbnm$ structure, represent a prototypical class of “improper ferroelectrics”,^{1–3} where electric dipoles are induced by a frustrated magnetic ordering. Among this family of compounds, TbMnO_3 and DyMnO_3 show non-collinear magnetic structures, where spin-orbit coupling (SOC) via the Dzyaloshinskii-Moriya (DM) interaction is responsible for the weak ferroelectric polarization ($P < 0.1 \mu\text{C}/\text{cm}^2$) and the magnetoelectricity.^{4,5} On the other hand, the onset of a ferroelectric state induced by an exchange-striction mechanism (such effect is often called “inverse Goodenough-Kanamori interaction”⁶) was theoretically proposed for HoMnO_3 in the antiferromagnetic E-type (AFM-E) spin configuration,^{7,8,10,11} and later experimentally confirmed.^{12–14} In the framework of the degenerate double exchange model,⁷ it has been shown that a *displacement mechanism*, based on the difference - in terms of bond-angles and bond-lengths - between Mn atoms with parallel and antiparallel spins, takes place for inequivalent bridge oxygens, leading to a net ferroelectric polarization (P) directed along the a axis. The mechanism was confirmed by a density functional theory (DFT) study,⁸ which also reported a comparable contribution arising from a purely *quantum mechanical mechanism*, resulting in a large value of the total ferroelectric polarization, $P \approx 6 \mu\text{C}/\text{cm}^2$. Further calculations based on the Heyd-Scuseria-Ernzerhof hybrid functional report a value of the ferroelectric polarization of $\approx 2 \mu\text{C}/\text{cm}^2$.⁹ Microscopically, the electronic contribution is explained

in terms of the asymmetric hopping of $\text{Mn-}e_g$ electrons between neighboring Mn ions, where the “one-way” direction of hopping is determined both by the orbital ordering and by the E-type spin configuration.¹⁰ As a second effect, the ions move to enhance the polarization induced by the asymmetric hopping; in fact, the Mn-O-Mn angle between the ferromagnetically coupled Mn spins increases after ferroelectric ionic relaxations, resulting in an increase of the e_g hopping integrals.

For an easier detection of the polarization in experiments, an increase of the polarization in this system is desired. A possible path to achieve this is by increasing the $\text{Mn-}e_g$ hopping amplitude by modulating the (ab) in-plane Mn-O-Mn bond angle ϕ (average value of $\phi=144^\circ$ for HoMnO_3 ¹⁵), as well as the Mn-O bond lengths. However, the enhancement of ϕ may lead, according to the Goodenough-Kanamori rule,¹⁶ to the stabilization of other magnetic phases, *i.e.* the non-collinear configuration, with a smaller P , observed in TbMnO_3 ($\phi=145^\circ$) and the paraelectric AFM-A phase in LaMnO_3 ($\phi=155^\circ$). Another possible recipe to increase the polarization P is to shorten the bond lengths in the AFM-E magnetic ground state, hopefully keeping the angle ϕ unchanged in such a way that the AFM-E phase does not turn unstable. In this context, here we theoretically investigate strain effects both on the magnetic configuration and on the polarization for orthorhombic HoMnO_3 , where the in-plane lattice constants a and b are artificially modified in order to mimic the compressive/tensile modes acting in thin films grown on different substrates.

II. STRUCTURAL AND COMPUTATIONAL DETAILS

Orthorhombic HoMnO_3 crystallizes in the $Pbnm$ structure (corresponding to $Pnma$ in the standard setting; in this paper, we chose c as the longest axis). Here, strong distortions with respect to the ideal cubic perovskite, *i.e.* GdFeO_3 type tilting of MnO_6 octahedral cages and Jahn-Teller (JT) distortions, stabilize the orbital ordering of $\text{Mn-}e_g^1$ states, where the orbital order is expressed as $(3x^2 - r^2)/(3y^2 - r^2)$. Although the hexagonal non-perovskite phase is more stable than the orthorhombic phase in HoMnO_3 , the transition to the metastable orthorhombic phase can be obtained by high-pressure synthesis.

DFT simulations were performed using the VASP code¹⁷ and the PAW pseudopotentials¹⁸ within the GGA formalism. (Note that for ortho- RMnO_3 , it is already known that the GGA+ U treatment¹⁹ worsens the agreement with experimental results compared to bare GGA, as regards the optimized atomic structure and the magnetic stabilization.^{10,20}) The cut-off energy for the plane-wave expansion of the wave-functions was set to 400 eV and a \mathbf{k} -point shell of (4, 2, 3) was used for the Brillouin zone integration according to the Monkhorst-Pack special point scheme. The in-plane lattice constants corresponding to the unstrained structure are taken as $a = 5.2572 \text{ \AA}$ and $b = 5.8354 \text{ \AA}$, equal to the experimental values.¹⁵ In order to mimic strain, these values were progressively changed from -4% (compressive strain) to 4% (tensile strain). The lattice constant c was optimized for each (a, b) value, as well as the internal coordinates. In the unstrained case, the theoretically optimized c is found to be equal to 7.3952 \AA , slightly underestimated compared to the experimental value of 7.3606 \AA . In the AFM-E magnetic configuration (AFM q vector along b), the unit cell is doubled along b (40 atoms/cell). Therefore, the crystal structure is optimized in the non-centrosymmetric $P2_1mn$ symmetry, allowing for a ferroelectric polarization along x (P_x). (Without spin-orbit coupling, the magnetic group is not considered.) A schematic representation of the structure in the AFM-E magnetic configuration is shown in Fig. 1. The electronic polarization $P_{\text{Berry}} = P_{\text{tot}}$ is calculated using the Berry phase method²¹ and compared to the classical point charge model (PCM) result, where $P_{\text{PCM}} = P_{\text{ion}}$ is calculated as the product of the nominal ionic valence and of the ionic displacements. In order to discuss the stability of different magnetic configurations, the internal atomic coordinates were fully optimized in the AFM-A configuration, characterized by in-plane ferromagnetic and inter-plane antiferromagnetic couplings. Using this relaxed centrosymmetric structure, the total energies of several magnetic configurations (antiferromagnetic AFM-A, AFM-C, AFM-G, AFM-E, AFM-E* and ferromagnetic FM configurations) were compared, and the exchange coupling integrals J_{ij} were calculated by mapping the system onto a Heisenberg model (see Ref. 10 for details).

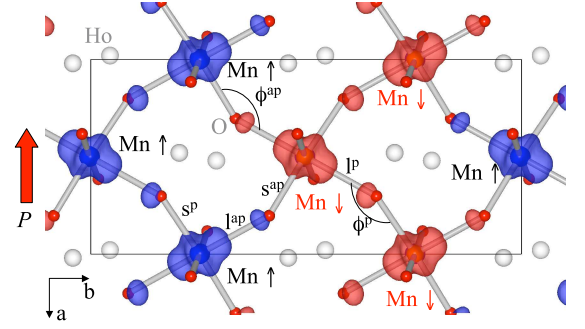


FIG. 1: (Color online) Spin density of the $\text{Mn-}e_g$ states (within an energy range up to 1 eV below the Fermi energy) in AFM-E configuration without strain, projected in the (ab) plane, referred in the text as *in-plane*. Blue (dark) and red (light) isosurface show up- and down-spin state (at $\pm 0.1 e^-$), respectively. Due to the exchange striction, the Mn-O-Mn bond angles ϕ^p between parallel-coupled Mn-spins and ϕ^{ap} between anti-parallel-coupled Mn-spins are different, as well as the Mn-O bond distances l^p , l^{ap} and s^p , s^{ap} . The direction of the net polarization ($P \parallel -a$) is denoted by a big red arrow.

III. STRAIN EFFECT ON ATOMIC STRUCTURE

Fig. 2 shows the dependence of the total energy on strain. The deviation from the origin of the energy minimum, giving an estimate of the error of bare GGA treatment with respect to experimental results, is less than 1% (rather typical for DFT calculations). The band gap, given by the JT-splitting of $\text{Mn-}e_g$ states, is also found to decrease under compressive strain in the (ab) plane.

In Fig. 3 and Fig. 4 we show how the change in the a and b lattice constants affects the optimized value of the lattice constant c and the lattice volume, as well as the Mn-O bond lengths and Mn-O-Mn bond angles in the AFM-E configuration. Under in-plane compressive strain, the c lattice constant is expanded, while the vol-

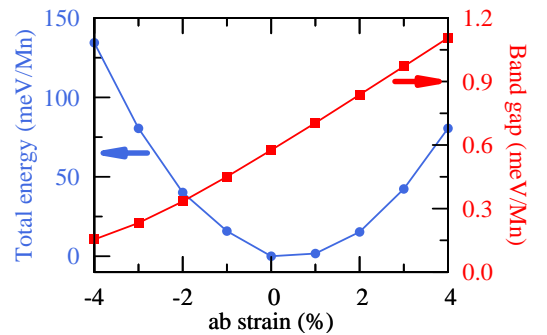


FIG. 2: (Color online) Calculated variation of the total energy difference and the band gap with optimized atomic structure in AFM-E configuration under in-plane strain.

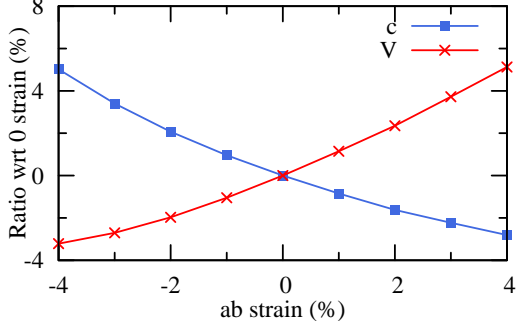


FIG. 3: (Color online) Calculated variation of equilibrium c and lattice volume V under in-plane strain, a and b being fixed for a given strain.

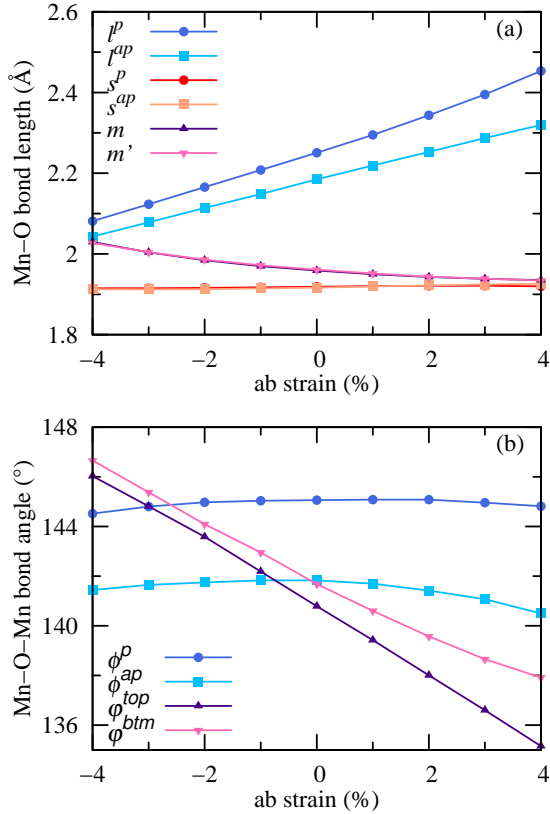


FIG. 4: (Color online) Variation of (a) the Mn-O bond lengths, in-plane l , s (long axis and short axis in JT-distorted MnO_6 octahedron) and inter-plane m and (b) the Mn-O-Mn in-plane bond angles ϕ and inter-plane bond angles φ in the AFM-E configuration under (ab) in-plane strain.

ume is contracted. The Mn-O bond lengths and the Mn-O-Mn bond angles depend on the relative alignment of the Mn spins, parallel or antiparallel, as a consequence of exchange striction. Remarkably, the in-plane bond angles, ϕ^p and ϕ^{ap} , are kept rather constant under strain, whereas the bond lengths are much more modulated.

The inter-plane Mn-O-Mn bond angles, ϕ^{top} and ϕ^{btm} , show a rapid increase under compressive strain. Recalling the fact that the hopping integral between Mn- e_g states depends both on the bond angle ϕ and on the bond length d — the overlap integral b is described as²³ $\tilde{b} = \cos((180^\circ - \phi)/2)/d^{3.5}$ —, apparently oxygen ions are displaced in such a way that the hopping energy is maximized. On the other hand, the difference $|\phi^p - \phi^{ap}|$ of the bond-angle between Mn ions with parallel and antiparallel spins (proven to be relevant for the ionic contribution to the polarization) slightly increases under tensile strain, probably because of the smaller elastic energy that binds oxygen atoms in a relatively larger space in the lattice. Such a reduction of the elastic energy is expected to enhance ionic displacement and, consequently, the ionic contribution to polarization, P_{ion} .

IV. MAGNETIC CONFIGURATION

In this section we focus on the magnetic stabilization under strain. As shown in Fig. 5, the AFM-E phase is stable under tensile strain, but, as a general trend, under compressive strain (at -4%) none of the AFM phases is any longer stable with respect to the ferromagnetic phase. This trend is consistent with the evolution of the band gap, which closes towards a metallic state under compressive strain. Specifically, the double exchange interaction between the Mn- e_g states is enhanced in this region of strain. In fact, the in-plane nearest-neighbor FM coupling $J_{\parallel}^{\text{nn}}$ progressively increases under compressive strain. The AFM-E configuration, gaining energy both from the double exchange interaction along the zigzag spin chains and from the ferroelectric ionic displacements, is more stable than the FM and AFM-A phases within a region of strain ranging from -3% to 4%. It is also worth noticing that the inter-plane next-neighbor coupling J_{\perp}^1 rapidly changes sign under compressive strain, turning from AFM to FM. The reason for the emergence of a FM inter-plane coupling will be explained in the next section. From the calculated exchange interactions, J_{ij} , we can also estimate the critical temperature T_c in the mean-field approximation for the Heisenberg model: we find that the Néel temperature for the AFM-E phase is $k_B T_N = 2/3(J_{\parallel}^{\text{nn}} + J_{\perp}^1)$ and that the Curie temperature is $k_B T_C = 2/3(2J_{\parallel}^{\text{nn}} + J_{\parallel}^{\text{nnn}} + J_{\perp}^1 + 4J_{\perp}^2)$ for the FM phase, with k_B the Boltzmann constant. Their dependence on strain is shown in Fig. 5.

V. FERROELECTRICITY AND JAHN-TELLER DISTORTION

Finally, we consider the strain effect on the ferroelectric polarization in the AFM-E phase. In order to discuss the evolution of P as a function of strain, we calculate the polarization also at -4% and -3% strain, where the AFM-E phase is not magnetically stable with respect to

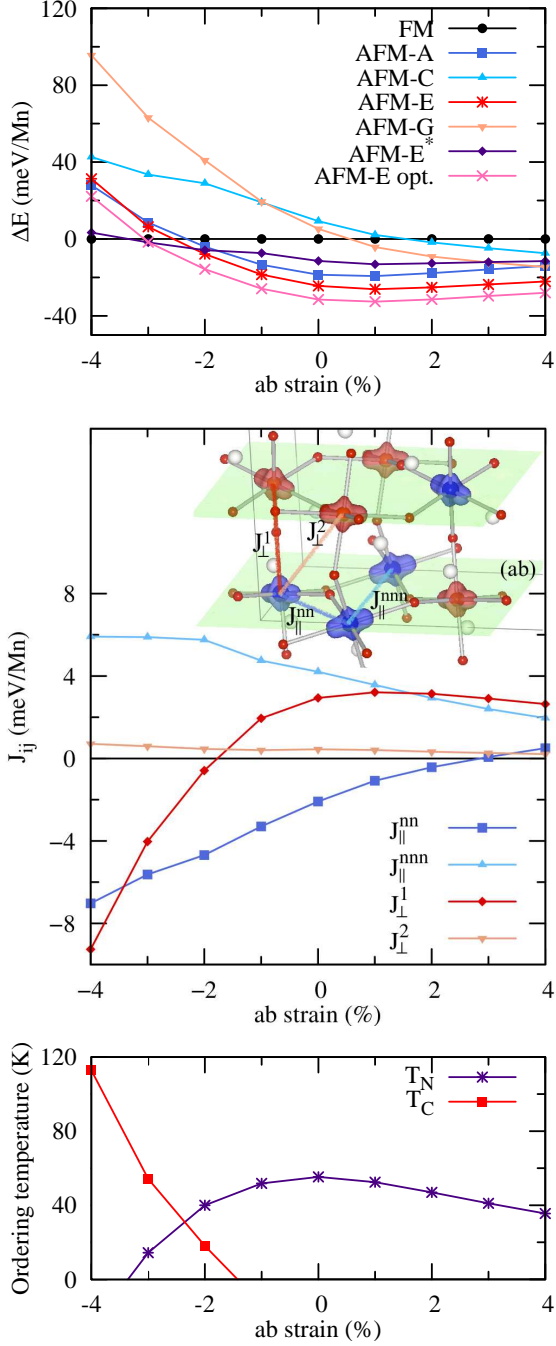


FIG. 5: (Color online) Variation of (a) magnetic stabilization (total energy of AFM-A, C, G, E and E* phases with respect to FM in the atomic structure fixed to the optimized AFM-A phase, and the total energy of the AFM-E phase for which the atomic structure was optimized in the non-centrosymmetric phase). (b) Interatomic exchange interaction (J_{ij}): The first nearest-neighbor in-plane J_{\parallel}^{nn} , next nearest-neighbor in-plane J_{\parallel}^{nnn} , first nearest-neighbor inter-plane J_{\perp}^1 , next nearest-neighbor inter-plane J_{\perp}^2 . Positive (negative) sign denotes AFM (FM) coupling. (c) Ordering temperatures of the FM and AFM-E phases within the mean-field approximation.

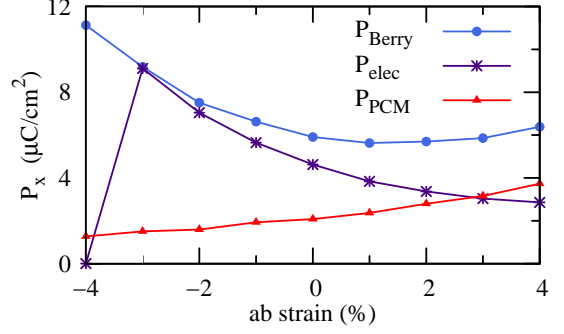


FIG. 6: (Color online) Variation of the ferroelectric polarization, P_{Berry} (electronic+ionic contribution) and P_{PCM} (ionic contribution), with strain.

the FM one. As shown in Fig. 6, interestingly, it turns out that P ($=P_{\text{Berry}}$) is enhanced at both limits of strain: *i.e.* under tensile strain, the contribution to P arising from ionic displacements ($=P_{\text{PCM}}$) increases, whereas the electronic contribution to P ($=P_{\text{Berry}}-P_{\text{PCM}}$) decreases, with an opposite trend in the opposite limit of compressive strain. The former trend is easily understood: in a larger space, oxygen ions are more freely displaced by the exchange striction, resulting in an enhancement of P_{ion} , as discussed in Sec. III. The latter is less easy to understand intuitively. One possibility is that the hopping of Mn- e_g electron increases due to the shorter bond length, so that the *asymmetric hopping* is increased, thus explaining the enhanced electronic contribution to the net polarization. In Fig. 7, the bandwidth w of Mn- e_g states, which reflects the hopping integral between Mn- e_g states at neighboring Mn-sites, is shown to be unchanged regardless of strain. However, the JT splitting is changed significantly, as one may have expected by looking at the trend of Mn-O bond lengths shown in Fig. 4, where the long axis l and short axis s get closer under compressive strain. Besides, at -4% of strain, l and m becomes similar, and as a consequence Q_3 changes sign from negative to positive, as shown in Fig. 8. This change of the JT distortion is reflected in the shape of the ordered orbitals. Figure 9 shows the change of the orbital shape under compressive strain. The $3x^2 - r^2$ orbital acquires additional character of the $x^2 - z^2$ orbital (in a local frame $x = l$, $y = s$, $z = m$). As a consequence of the orbital change, an inter-plane Mn-O bonding through e_g electrons is formed (c.f. small weight of the charge density on the apical oxygen atom in Fig. 9(a) but not in (b)); this might also be related to the fact that inter-plane magnetic coupling turns FM under compressive strain. Regarding the enhancement of the electronic contribution to P , we should consider the charge transfer caused by Mn electrons at occupied e_g state, which hop into unoccupied e_g state at neighboring Mn site. It is expected that the charge transfer is enhanced when the JT-splitting is small.

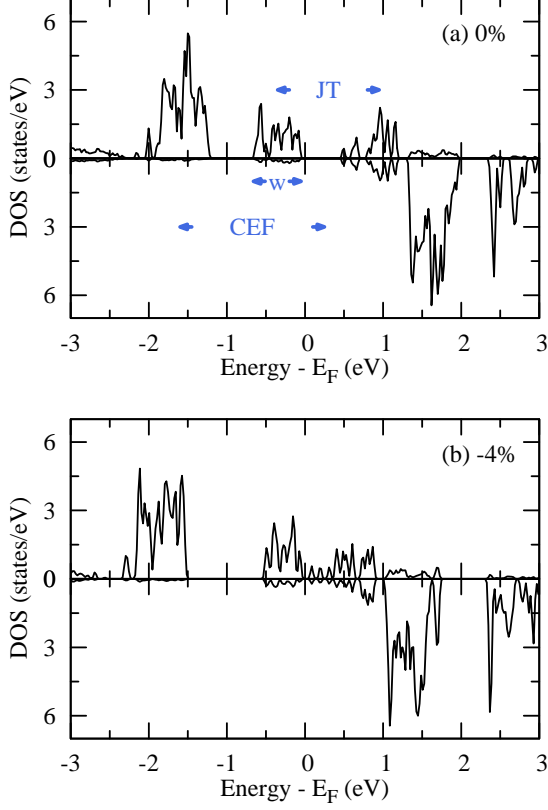


FIG. 7: Partial density of states (DOS) at Mn site under no strain and -4% strain. JT, w and CEF denote JT splitting at Mn- e_g state, band width (\propto hopping integral t) of e_g^1 occupied state, and crystal field splitting between e_g and t_{2g} states.

VI. MODEL HAMILTONIAN

The change in orbital ordering as a response to compressive strain found in the DFT framework can be accounted for in a model Hamiltonian approach. We consider a degenerate double exchange model, where infinite Hund coupling between the t_{2g} and the e_g electrons is assumed.²⁴ This allows us to neglect spin degrees of freedom of conduction electrons, which are fixed by the underlying magnetic structure of the core spins. In the E-type configuration, electrons can move along zig-zag chains on a background of parallel (ferromagnetically coupled) core spins, which experience an antiferromagnetic interchain coupling. Orbital ordering can then be stabilized by the Jahn-Teller coupling to the lattice. The Hamiltonian reads as:

$$H = - \sum_{\langle i,j \rangle} t_{ij}^{\alpha,\beta} \cos \Theta_{ij} c_{i\alpha}^\dagger c_{j,\beta} + J \sum_{\langle i,j \rangle} \mathbf{S}_i \cdot \mathbf{S}_j + E_{JT} \sum_i [2(q_{2i}\tau_{xi} + q_{3i}\tau_{zi}) + q_{2i}^2 + q_{3i}^2]. \quad (1)$$

We adopt the standard notation, with $c_{i\alpha}^\dagger$ ($c_{i\alpha}$) creation (annihilation) operators for electrons in the bands $\alpha =$

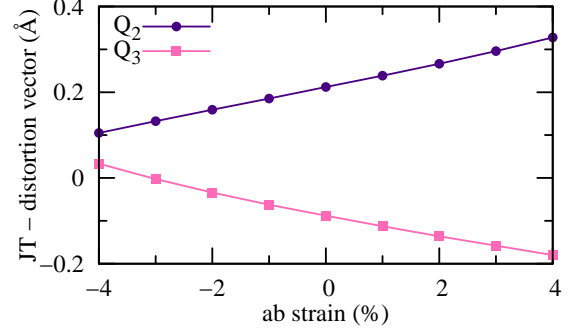


FIG. 8: (Color online) Variation of the Jahn-Teller vector $\mathbf{Q} = (Q_2, Q_3) \equiv \left(\frac{1}{\sqrt{2}}(l-s), \frac{1}{\sqrt{6}}(2m-l-s) \right)^{24}$ in the AFM-E configuration, where l , m and s are averaged, under in-plane strain.

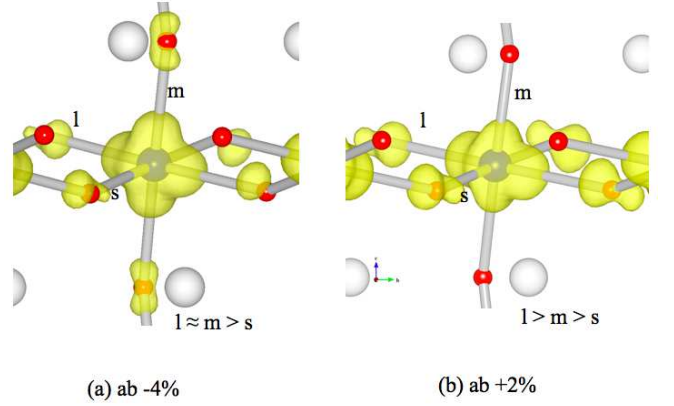


FIG. 9: (Color online) Isosurface of charge density of occupied Mn- e_g^1 state (within an energy range up to 1eV below Fermi energy) under (a) -4% and (b) +2% strain.

a, b (stemming respectively from $d_{x^2-y^2}$, $d_{3z^2-r^2}$ orbitals on Mn^{3+}); $t_{ij}^{\alpha,\beta}$ are the oxygen-mediated hopping amplitudes between nearest-neighbors manganese atoms, i.e. $t_{aa}^x = t_{aa}^y = 3t_0/4$, $t_{bb}^x = t_{bb}^y = t_0/4$, $t_{ab}^x = -t_{ba}^y = \sqrt{3}t_0/4$ with $t_0 = (pd\sigma)^2$ as the energy reference.²⁵ The Θ_{ij} are the angles between neighboring Mn-core spins S_i and S_j and J is the exchange coupling which they experience. The JT modes are expressed through the dimensionless q_{2i}, q_{3i} ($= (k/g) \mathbf{Q}_i$) and $E_{JT} = g^2/2k$ is the static Jahn-Teller energy; $\tau_{\mu i} = \sum_{\alpha\beta} c_{i\alpha}^\dagger \sigma_{\alpha\beta}^\mu c_{i,\beta}$ are the orbital pseudospins, where $\sigma_{\alpha\beta}^\mu$ are the Pauli matrices.

We evaluated the optimal q_{2i}, q_{3i} keeping the t_{2g} spins in E-type configuration, and we found that in the undoped case (one electron per Mn site) an orbital ordering occurs as soon as the JT coupling is large enough to induce a finite distortion. The character of orbitals involved in the ordered phase can be visualized by eval-

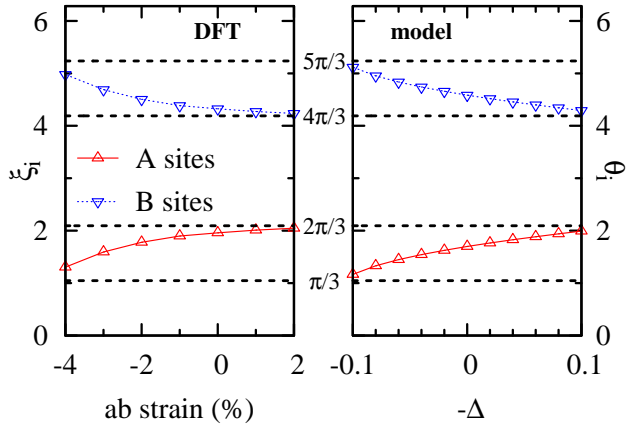


FIG. 10: (Color online) Jahn-Teller phase ξ_i at neighboring sites as a function of strain as obtained in DFT (left), compared with orbital phase θ_i evaluated in model Hamiltonian approach as a function of crystal field with reversed sign (right). Dotted lines at $\pi/3$ ($2\pi/3$) and $5\pi/3$ ($4\pi/3$) correspond to $x^2 - z^2$ ($3x^2 - r^2$) and $y^2 - z^2$ ($3y^2 - r^2$) orbitals respectively.

uating the average occupancy of the atomic orbitals, defined as $\rho_{\alpha i} = \langle \phi_{\alpha i}^\dagger \phi_{\alpha i} \rangle$, where $\phi_{\alpha i} = -\sin(\theta_i/2) c_{ai} + \cos(\theta_i/2) c_{bi}$ and α labels each of the possible e_g -electron orbitals with the corresponding angle θ_i (e.g. $\theta_i = 2\pi/3$ ($4\pi/3$) corresponds to $3x^2 - r^2$ ($3y^2 - r^2$) orbital, see for instance Ref. 24).

The effect of the in-plane strain can be mimicked by the introduction of a crystal-field term $+\Delta \sum_i \tau_{zi}$ in the Hamiltonian (1); if we consider a compression in the ab plane, then Δ should be chosen positive. Another effect of compression is of course to increase the elastic stiffness of MnO_6 octahedra, therefore one should expect a decrease of JT static energy (as indeed observed in the reduction of the JT gap found in DFT calculations). We found that, upon increasing Δ , the orbital ordering is not affected in its alternating pattern, but there is a change in the weight of involved atomic orbitals, namely the weight of $x^2 - z^2$ ($y^2 - z^2$) is increased with respect to $3x^2 - r^2$ ($3y^2 - r^2$). At the same time, the gap between the e_g -electron bands is reduced even with fixed JT coupling. To visualize the evolution of orbitals involved in the ordered pattern as a function of strain we can evaluate the angle $\theta_i = \tan^{-1}(\langle \tau_{xi} \rangle / \langle \tau_{zi} \rangle)$ and compare it with the Jahn-Teller phase $\xi_i = \tan^{-1}(Q_{2i}/Q_{3i})$ extrapolated from DFT calculations. As shown in Fig. 10, we find a good qualitative agreement between the two phases.

We have also checked our results by considering the effect of cooperative distortions of oxygens. This has been done by optimizing the Hamiltonian (1) with respect to oxygen displacements $\{u\}$ from their equilibrium positions rather than optimizing the local distortions of the MnO_6 octahedron labeled by $\{q\}$: in this case the strain can be mimicked by changing the equilibrium positions of oxygens, specifically decreasing the MnO distances in

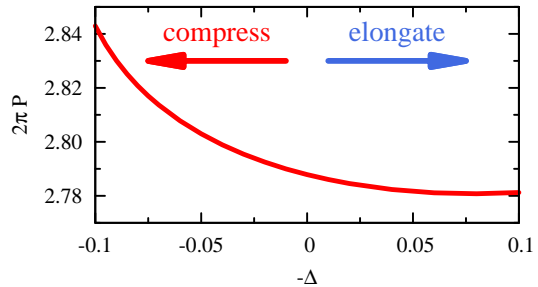


FIG. 11: (Color online) Electronic polarization as a function of $-\Delta$ (Δ is the crystal field).

the ab plane with respect to the equilibrium position of oxygens along the c axis. This approach provides results which are consistent with those obtained in the noncooperative treatment of Jahn-Teller effect.

We focus then on possible electronic polarization. Due to the AFM-E magnetic configuration, at $T = 0$ e_g electrons can only hop between sites with ferromagnetically aligned core-spins. This implies that hopping processes can occur only along one-dimensional zig-zag chains. As discussed in Ref. 26, the presence of Jahn-Teller centers in this one-dimensional system can induce a Berry phase in the Bloch function, intimately related to the orbital ordering induced by JT distortions, from which electronic polarization can be inferred. We follow the prescription described in Ref. 27 and evaluate the polarization within the chains as $P_{el} = \lim_{L \rightarrow \infty} \frac{e}{2\pi} \text{Im} \ln \langle \Psi_0 | e^{i \frac{2\pi}{L} \hat{X}} | \Psi_0 \rangle$, where L is the length of the one-dimensional chain (thermodynamic limit is taken at the end of the calculation), Ψ_0 is the ground-state wavefunction of model (1) with optimized q_{2i} , q_{3i} , and $\hat{X} = \sum_i i \hat{n}$ is the electronic position operator. The onset of the orbital ordering within the zigzag chains induces a finite polarization whose origin is fully electronic, the ions position being fixed in the system.²⁸ As shown in Fig. 11, we find that P_{el} is indeed enhanced by increasing Δ (i.e. as a consequence of a compressive strain in our model approach), in excellent qualitative agreement with the DFT results.

VII. CONCLUSIONS

The ferroelectric and magnetic properties of orthorhombic HoMnO_3 were investigated by a combined density functional theory and model Hamiltonian study. We found an increase in the electric polarization when the system is subjected to in-plane compressive strain. This is closely related to the modifications in the electronic structure, namely the orbital ordered states $3x^2 - r^2/3y^2 - r^2$ gain additional character of the $x^2 - z^2/y^2 - z^2$ states. Beside leading to an increase of the polarization, the orbital mixing influences the magnetic stability; thus, a crossover from the AFM-E to the FM phase occurs

around -3% compressive strain.

Acknowledgments

The research leading to these results has received funding from the European Research Council under the EU Seventh Framework Programme (FP7/2007-2013) / ERC grant agreement n. 203523. Computational support from

the Swedish National Infrastructure for Scientific Computing (SNIC), Caspur Supercomputing Center (Rome) and Cineca Supercomputing Center (Bologna) is gratefully acknowledged. B. S. acknowledges support from VR. O. E. acknowledges support from VR, SSF, ERC, and the European Commission, project number FP7-NMP-2008-EU-India2-233513. The charge density plots were performed using the program VESTA.²²

-
- * diana.iusan@spin.cnr.it
- ¹ S. W. Cheong and M. Mostovoy, *Nat. Mater.* **6**, 13 (2007).
 - ² A. P. Levanyuk and D. G. Sannikov, *Sov. Phys. Usp.* **17**, 199 (1974).
 - ³ M. Iizumi, J. D. Axe, G. Shirane and K. Shimaoka, *Phys. Rev. B* **15**, 4392 (1977).
 - ⁴ M. Kenzelmann, A. B. Harris, S. Jonas, C. Broholm, J. Schefer, S. B. Kim, C. L. Zhang, S.-W. Cheong, O. P. Vajk, and J. W. Lynn, *Phys. Rev. Lett.* **95**, 087206 (2005).
 - ⁵ I. A. Sergienko and E. Dagotto, *Phys. Rev. B* **73**, 094434 (2006).
 - ⁶ K. Yamauchi, S. Picozzi, *J. Phys. : Condens. Matter* **21**, 064203 (2009).
 - ⁷ I. A. Sergienko, C. Sen, and E. Dagotto, *Phys. Rev. Lett.* **97**, 227204 (2006).
 - ⁸ S. Picozzi, I. A. Sergienko, K. Yamauchi, B. Sanyal and E. Dagotto, *Phys. Rev. Lett.* **77**, 227201 (2007).
 - ⁹ A. Stroppa and S. Picozzi, *Phys. Chem. Chem. Phys.* **12**, 5405 (2010).
 - ¹⁰ K. Yamauchi, F. Freimuth, S. Blugel, and S. Picozzi, *Phys. Rev. B* **78**, 014403 (2008).
 - ¹¹ S. Picozzi and C. Ederer, *J. Phys.: Condens. Matter* **21**, 303201 (2009).
 - ¹² B. Lorenz, Y. Q. Wang, and C. W. Chu, *Phys. Rev. B* **76**, 104405 (2007).
 - ¹³ B. Lorenz, Y. Q. Wang, Y. Y. Sun, and C. W. Chu, *Phys. Rev. B* **70**, 212412 (2004).
 - ¹⁴ V. Yu. Pomjakushin, M. Kenzelmann, A. Donni, A. B. Harris, T. Nakajima, S. Mitsuda, M. Tachibana, L. Keller, J. Mesot, H. Kitazawa, and E. Takayama-Muromachi, *New J. Phys.* **11**, 043019 (2009).
 - ¹⁵ J. A. Alonso, M. J. Martinez-Lope, M. T. Casais, and M. T. Fernández-Daz, *Inorg. Chem.* **39**, 917 (2000).
 - ¹⁶ J. B. Goodenough, *Phys. Rev.* **100**, 564 (1955); J. Kanamori, *J. Phys. Chem. Solids* **10**, 87 (1959).
 - ¹⁷ G. Kresse and J. Furthmüller, *Phys. Rev. B* **54**, 11169 (1996).
 - ¹⁸ P. E. Blöchl, *Phys. Rev. B* **50**, 17953 (1994).
 - ¹⁹ V.I. Anisimov, F. Aryasetiawan and A.I. Lichtenstein, *J. Phys.: Cond. Mat.* **9**, 767 (1997).
 - ²⁰ S. Picozzi, K. Yamauchi, G. Bihlmayer, and S. Blügel, *Phys. Rev. B* **74**, 094402 (2006).
 - ²¹ R.D. King-Smith and D. Vanderbilt, *Phys. Rev. B* **47**, 1651 (1993); R. Resta, *Rev. Mod. Phys.* **66**, 899 (1994).
 - ²² K. Momma and F. Izumi, *J. Appl. Crystallogr.*, **41**, 653 (2008).
 - ²³ J.-S. Zhou and J. B. Goodenough, *Phys. Rev. Lett.* **96**, 247202 (2006).
 - ²⁴ E. Dagotto, T. Hotta, and A. Moreo, *Physics Reports* **344**, 1 (2001).
 - ²⁵ J. C. Slater and G. F. Koster, *Phys. Rev.* **94**, 1498 (1954).
 - ²⁶ H. Koizumi, T. Hotta and Y. Takada, *Phys. Rev. Lett.* **80**, 4518 (1998).
 - ²⁷ R. Resta, *Phys. Rev. Lett.* **80**, 1800 (1998).
 - ²⁸ P. Barone, K. Yamauchi, and S. Picozzi, arXiv:1009.3369v1.